Progress In Electromagnetics Research, PIER 34, 189–218, 2001

CONTRAST SOURCE INVERSION METHOD: STATE OF ART

P. M. van den Berg and A. Abubakar

Centre for Technical Geosciences
Delft University of Technology
Mekelweg 4, 2628 CD, Delft, The Netherlands

Abstract—We discuss the problem of the reconstruction of the profile of an inhomogeneous object from scattered field data. Our starting point is the contrast source inversion method, where the unknown contrast sources and the unknown contrast are updated by an iterative minimization of a cost functional. We discuss the possibility of the presence of local minima of the nonlinear cost functional and under which conditions they can exist. Inspired by the successful implementation of the minimization of total variation and other edge-preserving algorithms in image restoration and inverse scattering, we have explored the use of these image-enhancement techniques as an extra regularization. The drawback of adding a regularization term to the cost functional is the presence of an artificial weighting parameter in the cost functional, which can only be determined through considerable numerical experimentation. Therefore, we first discuss the regularization as a multiplicative constraint and show that the weighting parameter is now completely prescribed by the error norm of the data equation and the object equation. Secondly, inspired by the edge-preserving algorithms, we introduce a new type of regularization, based on a weighted L^2 total variation norm. The advantage is that the updating parameters in the contrast source inversion method can be determined explicitly, without the usual line minimization. In addition this new regularization shows excellent edge-preserving properties. Numerical experiments illustrate that the present multiplicative regularized inversion scheme is very robust, handling noisy as well as limited data very well, without the necessity of artificial regularization parameters.

1 Introduction

2 Notation and Problem Statement

3 Contrast Source Inversion Method
- 3.1 The Local Minima
- 3.2 Updating of the Contrast Sources
- 3.3 Updating of the Contrast
- 3.4 Total Variation as a Multiplicative Constraint
- 3.5 Weighted L^2 Total-Variation Factor

4 Root Test

5 Numerical Examples
- 5.1 Concentric Squares
- 5.2 'Austria' Profile
- 5.3 Extended 'Austria' Profile
- 5.4 'Finger' Profile

6 Conclusions

Acknowledgment

References

1. INTRODUCTION

A central problem in target identification, non-destructive testing, medical imaging and numerous other areas of application concerns the determination of the shape, location and constitutive parameters, such as complex index of refraction or local sound speed, of a object or local inhomogeneity from measurements of the scattered field, when the object is illuminated successively by a number of known incident electromagnetic or acoustic waves. This problem is nonlinear and ill-posed, but during the years useful reconstruction algorithms have been developed. Comprehensive overviews of several results are given by Chew [7], Lesselier and Duchêne [21], Colton *et al.* [8], and Sabatier [26] and Van den Berg [29]. Most of these algorithms make use of the domain integral equation for the field inside the scattering object as well as the related integral representation for the field outside the object. In many cases, the methods are iterative of nature and each iteration requires the solution of a forward or direct problem.

Inspired by the success of iterative solutions of the forward scattering problem, the modified gradient method was introduced by Kleinman and Van den Berg [17], where both the unknown field and

the unknown material contrast are updated simultaneously in each iteration. The method recasts the inverse problem as an optimization problem in which a cost functional is minimized. The cost functional consists of the superposition of the mismatch of the measured field data with the field scattered by an object with a particular contrast function and the error in satisfying the object equation, i.e., a system of integral equations for the field due to each excitation. The necessity of a full solution of a forward problem in each iteration is avoided by the simultaneous updates of the fields and the contrast. The modified gradient method was refined by Kleinman and Van den Berg [18, 19] and extended with a minimization of total variation [31] to become an efficient way of reconstructing a complex refraction of index.

The modified gradient method has opened the doors for further research and together with the source-type integral equation method introduced by Habashy *et al.* [14], it formed the base of the contrast source inversion (CSI) method [32]. The CSI algorithm is what Kohn and McKenney [20] call an alternating direction implicit (ADI) method, wherein two sequences of variables, in the CSI method the contrast sources and the contrast itself, are iteratively reconstructed by alternately updating the sources and the contrast. This is contrary to the modified gradient method, where the fields and the contrast are updated simultaneously. Similar to the modified gradient method, in each iteration there is no full inversion of the object equations involved. The CSI method outperforms the modified gradient method, because it is computationally faster, has less memory as well as data requirements and accommodates easily *a priori* information, see e.g., [1].

Although the addition of the total variation to the cost functional has a very positive effect on the quality of the reconstructions for both 'blocky' and smooth profiles, a drawback is the presence of an artificial weighting parameter in the cost functional, which can only be determined through considerable numerical experimentation and *a priori* information of the desired reconstruction. In [30], it was suggested to include the total variation as a multiplicative constraint, with the result that the original cost functional is the weighting parameter of the regularizer, so that this parameter is determined by the inversion procedure itself. This eliminates the choice of the artificial regularization parameters completely. The multiplicative type of regularization seems to handle noisy as well as limited data in a robust way without the usually necessary *a priori* information.

In the present paper, we investigate the occurrence of local minima in the CSI method. It is demonstrated that a sufficient number of illuminations may guarantee the convergence to the desired global minimum. In addition we introduce a simplified regularization factor,

viz., a weighted total-variation factor, as multiplicative constraint. Although it is an L^2-norm of the contrast gradient, it exhibits excellent edge-preserving properties. Since we use conjugate gradient directions for the contrast sources and the contrast, a second advantage is that the usual line minimization to determine the update parameters is avoided. This new multiplicative regularized CSI method is denoted as MR-CSI method.

From our numerical experiments we observe that the multiplicative regularized MR-CSI method seems to be a robust optimization method, both for noisy and limited data, avoiding the choice of the regularization parameters and hence avoiding the need of the necessary *a priori* information about which kind of reconstruction image is acceptable.

2. NOTATION AND PROBLEM STATEMENT

To illustrate the inversion method, we consider the theoretical model of the two-dimensional inverse scattering problem, with a bounded, simply connected, inhomogeneous object domain D in an unbounded homogeneous background medium. The object domain D embeds a scattering object (or objects) B, of which location and index of refraction (or contrast) are unknown. The vectors $\boldsymbol{p}$ and $\boldsymbol{q}$ denote the vectorial position in $\mathbb{R}^2$. To reconstruct the contrast function of the unknown objects, we assume that the scatterers are illuminated successively by a number of incident waves of one single frequency, $u_j^{\mathrm{inc}}(\boldsymbol{p}) = u^{\mathrm{inc}}(\boldsymbol{p}, \boldsymbol{q}_j)$, $j = 1, \ldots, J$, and source points $\boldsymbol{q}_j$ ($\boldsymbol{q}_j$ is replaced by the unit vector $\hat{\boldsymbol{q}}_j$ for plane waves). The sources are located in a domain (or on a curve) S outside of and surrounding D, where the measurement of the scattered field is made as well. We use the complex time factor $\exp(-\mathrm{i}\omega t)$, where ω is the radial frequency.

It has been shown that for a large class of scattering problems the total field in D satisfies the domain integral equation, see e.g., Colton and Kress [9],

$$u_j(\boldsymbol{p}) = u_j^{\mathrm{inc}}(\boldsymbol{p}) + k_{\mathrm{b}}^2 \int_D G(\boldsymbol{p}, \boldsymbol{q})\, \chi(\boldsymbol{q})\, u_j(\boldsymbol{q})\, \mathrm{dv}(\boldsymbol{q})\,, \quad \boldsymbol{p} \in D\,, \tag{1}$$

where $G(\boldsymbol{p}, \boldsymbol{q})$ denotes the Green function of the background medium,

$$G(\boldsymbol{p}, \boldsymbol{q}) = (\mathrm{i}/4) H_0^{(1)}(k_{\mathrm{b}} |\boldsymbol{p} - \boldsymbol{q}|)\,, \tag{2}$$

with $H_0^{(1)}$ the zero-order Hankel function of the first kind and the contrast

$$\chi(\boldsymbol{q}) = k^2(\boldsymbol{q})/k_{\mathrm{b}}^2 - 1\,, \tag{3}$$

where k_b is the wavenumber of the homogeneous embedding and $k(\boldsymbol{q})$ the wavenumber of the scattering object. Note that if $\boldsymbol{q}$ is not in B, the contrast function χ vanishes outside B. Now, with (1) the scattered field is defined as

$$u_j^{sct}(\boldsymbol{p}) = u_j(\boldsymbol{p}) - u_j^{\mathrm{inc}}(\boldsymbol{p}) = k_\mathrm{b}^2 \int_D G(\boldsymbol{p},\boldsymbol{q})\,\chi(\boldsymbol{q})\,u_j(\boldsymbol{q})\,\mathrm{dv}(\boldsymbol{q})\,. \tag{4}$$

If the total field u_j is known, the scattered field u_j^{sct} can be calculated with the help of (4). We are then able to calculate the scattered field in the domain S. Because we measure the scattered field in the domain S, which is outside D where the contrast function χ vanishes, the right-hand side of (4) is equal to $f_j(\boldsymbol{p})$, i.e.,

$$f_j(\boldsymbol{p}) = k_\mathrm{b}^2 \int_D G(\boldsymbol{p},\boldsymbol{q})\,\chi(\boldsymbol{q})\,u_j(\boldsymbol{q})\,\mathrm{dv}(\boldsymbol{q})\,, \quad \boldsymbol{p}\in S\,, \tag{5}$$

if the measurements are noise- and error-free. This last assumption is unlikely and therefore the so-called data equations (5) do not hold exactly. Equations (1) and (5) are two equations from which the fields u_j and contrast χ have to be determined. This problem is nonlinear and has to be solved iteratively. In the modified gradient methods [17–19], the necessity of a full solution of the forward problem of equation (1) in each iteration is avoided by treating equations (1) and (5) as a system of equations and a functional combining these equations is minimized by updating the fields and contrast simultaneously in conjugate directions.

However, in the CSI method it is observed that the data equations contain the unknown field inside the scattering object and the contrast in the form of a product; it can be written as a single quantity, viz. the contrast source

$$w_j(\boldsymbol{p}) = \chi(\boldsymbol{p})\,u_j(\boldsymbol{p})\,, \tag{6}$$

which can be considered as an equivalent source that produces the measured scattered field, since the field u_j satisfies the equation

$$(\nabla^2 + k_\mathrm{b}^2)u_j(\boldsymbol{p}) = -k_\mathrm{b}^2 w_j(\boldsymbol{p}), \qquad \boldsymbol{p}\in B. \tag{7}$$

Multiplying both sides of (1) with χ, and using (6), we define in symbolic form the object or state equations as

$$w_j = \chi u_j^{\mathrm{inc}} + \chi G_D w_j\,, \quad \boldsymbol{p}\in D\,, \tag{8}$$

and the data equations (5) as

$$f_j = G_S w_j\,, \quad \boldsymbol{p}\in S\,, \tag{9}$$

where the subscripts D and S on the operators, defined implicitly in (1) and (5), are added to accentuate the location of the point $\boldsymbol{p}$, since the operators are identical in all other respects, viz.

$$G_{D,S} w_j = k_b^2 \int_D G(\boldsymbol{p}, \boldsymbol{q})\, w_j(\boldsymbol{q})\, \mathrm{dv}(\boldsymbol{q})\,, \qquad \boldsymbol{p} \in D \text{ or } \boldsymbol{p} \in S\,. \tag{10}$$

We consider equations (8) and (9) as two equations from which we want to determine the unknown contrast sources $w_j(\boldsymbol{p})$ and the unknown contrast $\chi(\boldsymbol{p})$ in D.

3. CONTRAST SOURCE INVERSION METHOD

The CSI method recasts the inversion problem as a minimization of a cost functional, being a linear combination of errors in the data equation and the object equation. Assuming that w_j and χ represent an approximate solution of our inverse problem, the cost functional is defined as

$$F(w_j, \chi) = \eta_S \textstyle\sum_j \| f_j - G_S w_j \|_S^2 + \eta_D \sum_j \| \chi u_j^{\mathrm{inc}} - w_j + \chi G_D w_j \|_D^2\,, \tag{11}$$

where $\| \cdot \|_S^2$ and $\| \cdot \|_D^2$ denote the norms on $L^2(S)$ and $L^2(D)$, respectively. the positive normalization factors η_S and η_D has to be chosen appropriately. This will be discussed later. The first term measures the error in the data equation given in (9) and the second term measures the error in the object equation given in (8). This is a quadratic functional both in w_j and in χ, but the term $\chi G_D w_j$ is responsible for the nonlinearity of the inverse problem. Before we discuss the algorithm to solve for the contrast sources, w_j, and the contrast, χ, we first concentrate on the nonlinearity of the functional. We carry out an analysis similar to the one given by Isernia *et al.* [16] for the cost functional introduced in the modified gradient method.

3.1. The Local Minima

As the functional of (11) is a non-quadratic functional of the unknowns w_j and χ, the problem arises how to find its global minimum, assuming that there exists an unique one. In view of the large number of unknowns, globally effective minimization schemes are not feasible, while a gradient-based minimization scheme could be trapped into local minima, which are false solutions of our inverse problem. However, our cost functional at hand is a polynomial of fourth degree in terms of the unknowns. Let we assume that the contrast sources w_j^{exact} and the contrast χ^{exact} represent the exact solution of our inverse problem.

The contrast sources and the contrast can be written as a linear combination of the exact solution and some generic direction, viz.,

$$\begin{pmatrix} w_1(\boldsymbol{p}) \\ w_2(\boldsymbol{p}) \\ \cdot \\ \cdot \\ \cdot \\ \chi(\boldsymbol{p}) \end{pmatrix} = \begin{pmatrix} w_1^{\text{exact}}(\boldsymbol{p}) \\ w_2^{\text{exact}}(\boldsymbol{p}) \\ \cdot \\ \cdot \\ \cdot \\ \chi^{\text{exact}}(\boldsymbol{p}) \end{pmatrix} + \beta \begin{pmatrix} \Delta w_1(\boldsymbol{p}) \\ \Delta w_2(\boldsymbol{p}) \\ \cdot \\ \cdot \\ \cdot \\ \Delta\chi(\boldsymbol{p}) \end{pmatrix}. \tag{12}$$

Without loss of generality, we can take β to be real valued. Substituting (12) into the cost functional (11) and using the fact that the individual terms of the right-hand side of (11) vanish for the exact solution, we end up with the polynomial of fourth degree,

$$F(w_j, \chi) = \beta^2(A_D\beta^2 + 2B_D\beta + C_S + C_D)\,, \tag{13}$$

where

$$A_D = \eta_D \textstyle\sum_j \|\Delta\chi G_D \Delta w_j\|_D^2\,, \tag{14}$$

$$B_D = \eta_D \mathrm{Re} \textstyle\sum_j \langle \Delta\chi G_D \Delta w_j\,,\, \Delta\chi u_j^{\text{exact}} - \Delta w_j + \chi^{\text{exact}} G_D \Delta w_j \rangle_D\,, \tag{15}$$

$$C_D = \eta_D \textstyle\sum_j \|\Delta\chi u_j^{\text{exact}} - \Delta w_j + \chi^{\text{exact}} G_D \Delta w_j\|_D^2\,, \tag{16}$$

$$C_S = \eta_S \textstyle\sum_j \|G_S \Delta w_j\|_S^2\,, \tag{17}$$

and

$$u_j^{\text{exact}} = u_j^{\text{inc}} + G_D w_j^{exact}\,. \tag{18}$$

Since the derivative of (13) with respect to β is a cubic equation, we observe that, for a given generic direction $\{\Delta w_j\,(j = 1, 2, \ldots), \Delta\chi\}$, there are only two minima, viz., the global one and a local one. Now, a sufficient condition for (13) to have no local minimum other than the global one ($\beta = 0$) is that

$$\frac{B_D^2}{A_D(C_S + C_D)} < \frac{8}{9}\,. \tag{19}$$

In view of Schwarz equality we note that $B_D^2 \leq A_D C_D$, and as a consequence we certainly know that

$$\frac{B_D^2}{A_D(C_S + C_D)} \leq 1\,. \tag{20}$$

In view of (20) the condition for absence of local minima can be satisfied when

$$\frac{C_D}{C_S + C_D} < \frac{8}{9}\,. \tag{21}$$

When Δw_j are non-radiating contrast sources, i.e., $\sum_j \|G_S \Delta w_j\|_S^2 = 0$, this condition cannot be met. Further, when we take the normalization factor in C_D too large with respect to the normalization factor in C_S, there is major chance that we violate this condition as well. Therefore we return to condition (19) and our strategy to avoid local minima is to reduce the value of the left-hand side of (19) by taking enough excitations. As long as the quantities $\Delta\chi G_D \Delta w_j$ and $\Delta\chi u_j^{\text{exact}} - \Delta w_j + \chi^{\text{exact}} G_D \Delta w_j$ have different phase distributions, the terms of the summation over the excitations (j) in B_D can cancel destructively each other, while the terms in C_D are positive and add constructively. Hence, increasing the number of excitations may reduce the chance of being trapped in a local minimum. Later, for some representative examples, we shall investigate this phenomenon.

We first discuss an algorithm to solve for the contrast sources and the contrast. The CSI method constructs alternatively sequences of contrast sources $w_{j,n}$ by a conjugate gradient iterative method such that the contrast sources minimize the cost functional, and the contrast χ_n is then determined to minimize the error in the object equation. In each iteration, we search for an improved update of the contrast sources $w_j = w_{j,n}$ and the contrast $\chi = \chi_n$ by some minimization of the cost functional

$$F_n(w_j, \chi) = F_S(w_j) + F_{D,n}(w_j, \chi)\,, \tag{22}$$

with

$$F_S(w_j) = \eta_S \textstyle\sum_j \|f_j - G_S w_j\|_S^2\,, \tag{23}$$

$$F_{D,n}(w_j, \chi) = \eta_{D,n} \textstyle\sum_j \|\chi u_j^{\text{inc}} - w_j + \chi G_D w_j\|_D^2\,, \tag{24}$$

where the normalization factors are chosen as

$$\eta_S = \left(\textstyle\sum_j \|f_j\|_S^2\right)^{-1} \qquad \text{and} \qquad \eta_{D,n} = \left(\textstyle\sum_j \|\chi_{n-1} u_j^{\text{inc}}\|_D^2\right)^{-1}\,. \tag{25}$$

3.2. Updating of the Contrast Sources

The CSI method starts with the updating of the contrast sources w_j in the following manner. Define the data error to be

$$\rho_{j,n} = f_{j,n} - G_S w_{j,n}\,, \tag{26}$$

and the object error to be

$$r_{j,n} = \chi_n u_j^{\text{inc}} - w_{j,n} + \chi_n G_D w_{j,n}\,, \tag{27}$$

Now suppose $w_{j,n-1}$ and χ_{n-1} are known. We update w_j by

$$w_{j,n} = w_{j,n-1} + \alpha_n^w v_{j,n}\,, \tag{28}$$

where α_n^w is a real constant parameter and the update directions $v_{j,n}$ are functions of position.

The update directions are chosen to be the Polak-Ribière conjugate gradient directions, which search for improved directions when a change with respect to the directions of the last iteration occurs and restart the optimization when practically no changes are made in the subsequent gradients. These update directions are obtained by

$$v_{j,0} = 0\,, \qquad v_{j,n} = g_{j,n}^w + \frac{\mathrm{Re}\sum_k \langle g_{k,n}^w, g_{k,n}^w - g_{k,n-1}^w\rangle_D}{\sum_k \langle g_{k,n-1}^w, g_{k,n-1}^w\rangle_D} v_{j,n-1}\,, \quad n \geq 1\,, \tag{29}$$

where $g_{j,n}^w$ is the gradient of the cost functional with respect to w_j evaluated at $w_{j,n-1}$ and χ_{n-1}. Explicitly, the gradient for the updating of the contrast source is found to be

$$g_{j,n}^w = -\eta_S G_S^\star \rho_{j,n-1} - \eta_{D,n}\left[r_{j,n-1} - G_D^\star(\overline{\chi}_{n-1} r_{j,n-1})\right]. \tag{30}$$

In (30), $G_S^\star$ and $G_D^\star$ are the adjoints of G_S and G_D mapping $L^2(S)$ into $L^2(D)$ and $L^2(D)$ into $L^2(D)$, respectively. They are given by

$$G_S^\star \rho_{j,n-1} = \overline{k_\mathrm{b}^2} \int_S \overline{G(\boldsymbol{p},\boldsymbol{q})}\, \rho_{j,n-1}(\boldsymbol{q})\, dv(\boldsymbol{q}), \quad \boldsymbol{p} \in D\,, \tag{31}$$

and

$$G_D^\star(\overline{\chi}_{n-1} r_{j,n-1}) = \overline{k_\mathrm{b}^2} \int_D \overline{G(\boldsymbol{p},\boldsymbol{q})}\, (\overline{\chi}_{n-1} r_{j,n-1})(\boldsymbol{q})\, dv(\boldsymbol{q}), \quad \boldsymbol{p} \in D\,. \tag{32}$$

Here, the overbar denotes complex conjugate.

With the update directions completely specified, the real parameter α_n^w in (28) is determined as

$$\alpha_n^w = \underset{\text{real } \alpha}{\arg\min} \left\{F_S(w_{j,n-1} + \alpha\, v_n) + F_{D,n}(w_{j,n-1} + \alpha\, v_n, \chi_{n-1})\right\}, \tag{33}$$

and is found explicitly to be

$$\alpha_n^w = \frac{-\mathrm{Re}\sum_j \langle g_{j,n}^w, v_{j,n}\rangle_D}{\eta_S \sum_j \|G_S v_{j,n}\|_S^2 + \eta_{D,n} \sum_j \|v_{j,n} - \chi_{n-1} G_D v_{j,n}\|_D^2}\,. \tag{34}$$

At this stage, all quantities to update the contrast sources, see (28), are known and $w_{j,n}$ can be calculated.

The starting values for $w_{j,0}$ must still be chosen. Observe that we cannot start with $w_{j,0} = 0$ and $\chi_0 = 0$, since then the cost functional

(11) is undefined for $n = 1$. Therefore we choose as starting values the contrast sources that minimize the data error, which are the contrast sources obtained by back propagation,

$$w_{j,0}^{\text{bp}} = \frac{\|G_S^\star f_j\|_D^2}{\|G_S G_S^\star f_j\|_S^2} G_S^\star f_j. \tag{35}$$

The choice of the initial estimate and the updating of the contrast is discussed in the next subsection.

3.3. Updating of the Contrast

Before updating the contrast, we first define the updated field as

$$u_{j,n} = u_j^{\text{inc}} + G_D w_{j,n}\,. \tag{36}$$

Since the contrast only occurs in the second term of our cost functional, the contrast $\chi = \chi_n$ is obtained as minimizer of the cost functional

$$F_{D,n}(w_{j,n}, \chi) = \eta_{D,n} \textstyle\sum_j \|\chi u_{j,n} - w_{j,n}\|_D^2\,, \tag{37}$$

which is the normalized norm of the error in the object equation after updating the contrast sources to $w_{j,n}$, cf. (24). Without any *a priori* information, this norm is minimized when

$$\chi_n = \frac{\sum_j w_{j,n}\overline{u}_{j,n}}{\sum_j |u_{j,n}|^2}\,. \tag{38}$$

Note that this result is identical to the result obtained by updating the contrast as

$$\chi_n = \chi_{n-1} + \alpha_n^\chi d_n\,, \tag{39}$$

where $\alpha_n^\chi = \eta_{D,n}^{-1}$ and d_n is the preconditioned gradient of $F_{D,n}(w_{j,n}, \chi_{n-1})$, viz.,

$$d_n = \eta_{D,n} \frac{\sum_j (w_{j,n} - \chi_{n-1} u_{j,n})\overline{u}_{j,n}}{\sum_j |u_{j,n}|^2}\,. \tag{40}$$

In case we have *a priori* information that the real part and/or the imaginary part of the contrast is positive, we remark that this positivity constraint is easily implemented by enforcing a negative value to zero after each update of the contrast. Numerical experiments have shown that this simple adjustment leads to reconstruction results, which are very similar to the ones of the original CSI method with positivity constraint [32]. In all numerical examples presented later in this paper, we have enforced positivity.

As far as the starting value χ_0 is concerned, we start with the initial estimates $w_{j,0}^{\rm bp}$ of (35), compute the initial field $u_{j,0}$ using (36), to obtain, cf. (38),

$$\chi_0 = \frac{\sum_j w_{j,0}^{\rm bp} \overline{u}_{j,0}}{\sum_j |u_{j,0}|^2}\,, \quad \text{with } u_{j,0} = u_j^{\rm inc} + G_D w_{j,0}^{\rm bp}\,. \tag{41}$$

This completes the description of our non-regularized version of the contrast source inversion algorithm, where, in each iteration, we update the contrast sources followed by an update of the contrast. We remark that in a similar way as in the modified gradient method where the fields and the contrast are updated simultaneously, we have also modified our present CSI method by using a simultaneous update of the contrast sources and the contrast. After determination of the Polak-Ribière conjugate gradient directions for the contrast sources and contrast we minimize the cost functional for variation of the two complex parameters α_n^w and α_n^χ. This more complicated scheme yielded no significant improvement.

3.4. Total Variation as a Multiplicative Constraint

Recent work with image enhancement has shown that minimization of the total variation of the image can be a very useful approach, see e.g., [3, 5, 11, 12, 25, 33]. Van den Berg and Kleinman [31] incorporated the total variation (TV) in an inverse scattering problem by enhancing the modified gradient algorithm. In the latter approach a total variation term was added to the cost functional resulting in a substantial improvement of the performance of the reconstruction method, both for 'blocky' and smooth contrast configurations. The addition of the total variation to the cost functional has a very positive effect on the quality of the reconstructions for both 'blocky' and smooth profiles, but a drawback is the presence of an artificial weighting parameter in the cost functional, which can only be determined through considerable numerical experimentation [15] and *a priori* information of the desired reconstruction.

Van den Berg *et al.* [30] have suggested to include the total variation as a multiplicative constraint, with the result that the original cost functional is the weighting parameter, i.e., determined by the inversion problem itself. This eliminates the choice of the artificial regularization parameters completely. In each iteration, a multiplicative cost functional is introduced as

$$\mathcal{F}_n(w_j, \chi) = [F_S(w_j) + F_{D,n}(w_j, \chi)]\, F_n^{\rm TV}(\chi)\,, \tag{42}$$

where the first factor is the original cost functional (22) of the CSI method and where the second factor, the so-called TV-factor is given

$$F_n^{\mathrm{TV}}(\chi) = \frac{\displaystyle\int_D \left(|\nabla\chi(\boldsymbol{q})|^2 + \delta_{n-1}^2\right)^{\frac{p}{2}} \mathrm{dv}(\boldsymbol{q})}{\displaystyle\int_D \left(|\nabla\chi_{n-1}(\boldsymbol{q})|^2 + \delta_{n-1}^2\right)^{\frac{p}{2}} \mathrm{dv}(\boldsymbol{q})}\,, \tag{43}$$

Here, δ^2 is chosen as

$$\delta_{n-1}^2 = F_{D,n-1}\,\tilde{\Delta}^2\,, \tag{44}$$

where $\tilde{\Delta}$ denotes the reciprocal mesh size of the discretized domain D and $F_{D,n-1}$ is the normalized norm of the object error of the previous iteration, cf. (37). The new cost functional (42) is based on two things: the objective of minimizing the error in the data and object equations and the observation that the TV-factor, when minimized, converges to 1. The structure of the new cost functional is such that it will minimize the total variation with a large weighting parameter in the beginning of the optimization process, because the value of $F(w_{j,n}, \chi_n)$ is still large, and that it will gradually minimize more and more the error in the data and object equations when the total variation has reached a nearly constant value close to 1. The factor δ_{n-1}^2 is introduced for restoring differentiability. Its choice is inspired by the idea that in the first few iterations, we do not need the minimization of the total variation and as the iterations proceed we want to increase the effect of the total variation.

If noise is present in the data, the data error term will remain at a large value during the optimization and therefore, the weight of the total variation factor will be more significant. Hence, the noise will, at all times, be suppressed in the reconstruction process and we automatically fulfill the need of a larger TV-regularization when the data contains noise as suggested by Chan and Wong [6] and Rudin *et al.* [25].

The value p is often chosen to be either one or two. If $p = 1$ the L^1-norm in the TV-factor will try to make the contrast piecewise constant and therefore 'blocky' contrast can be reconstructed. However, when $p = 2$ (L^2-norm in the TV-factor), a smooth profile is favored.

By introducing this cost functional $\mathcal{F}_n$, the TV-factor does not change the updating of the contrast sources $w_{j,n}$ and the fields $u_{j,n}$, because $F_n^{\mathrm{TV}}(\chi_{n-1}) = 1$ at the beginning of each iteration.

The updating scheme for χ_n is given by

$$\chi_n = \chi_{n-1} + \alpha_n^{\chi} d_n\,, \tag{45}$$

where the update directions d_n are taken as Polak-Ribière conjugate gradient directions of the cost functional (42), viz.,

$$d_0 = 0\,, \qquad d_n = g_n^\chi + \frac{\mathrm{Re}\langle g_n^\chi, g_n^\chi - g_{n-1}^\chi\rangle_D}{\langle g_{n-1}^\chi, g_{n-1}^\chi\rangle_D} d_{n-1} \quad n \geq 1\,, \tag{46}$$

while the preconditioned gradient is determined as, cf. (40),

$$g_n^\chi = \frac{\eta_{D,n}[\sum_j (w_{j,n} - \chi_{n-1} u_{j,n})\overline{u}_{j,n}] + [F_S(w_{j,n}) + F_{D,n}(w_{j,n}, \chi_{n-1})]\, g_n^{\mathrm{TV}}}{\sum_j |u_{j,n}|^2}, \tag{47}$$

where

$$g_n^{\mathrm{TV}}(\boldsymbol{q}) = \frac{\dfrac{p}{2}\nabla \cdot \left[\dfrac{\nabla \chi_{n-1}(\boldsymbol{q})}{\left(|\nabla \chi_{n-1}(\boldsymbol{q})|^2 + \delta_{n-1}^2\right)^{1-\frac{p}{2}}}\right]}{\displaystyle\int_D \left(|\nabla \chi_{n-1}(\boldsymbol{q})|^2 + \delta_{n-1}^2\right)^{\frac{p}{2}} \mathrm{dv}(\boldsymbol{q})}\,. \tag{48}$$

Note that the gradient tends to the direction d_n of (40) of the original CSI method as the gradient, g_n^{TV}, tends to zero. The weighting of the gradients clearly depends on the errors in the cost functional F_S and $F_{D,n}$ and the TV-factor F_n^{TV}. Since we have a multiplicative cost functional, one can expect a higher nonlinear functional, but the gradient of this cost functional has the same form as the gradient of an additive cost functional with a weighting parameter related to $F_S + F_{D,n}$. Similar to an additive regularization, the present multiplicative regularization decreases the chance that the gradient has a zero direction, which reduces the possibility to arrive at in a local minimum.

With the Polak-Ribière update directions completely specified, the real-valued constant α_n^χ in (45) is found as

$$\alpha_n^\chi = \underset{\text{real } \alpha}{\arg\min}\{[F_S(w_{j,n}) + F_{D,n}(w_{j,n}, \chi_{n-1} + \alpha d_n)] F_n^{\mathrm{TV}}(\chi_{n-1} + \alpha\, d_n)\}. \tag{49}$$

When $p = 2$, we end up with a polynomial of fourth degree in α and its minimizer can be determined analytically. However, for $p = 2$ the reconstructed contrast is too smooth. For $p = 1$, the reconstruction is significantly improved, but the drawback is that the minimization can not be carried out analytically and the minimizing value of α_n^χ must be determined by a numerical line minimization. In the next subsection we therefore discuss a new TV-factor that has not only the advantages of an improved reconstruction of 'blocky' and smooth profiles, but in addition the advantage that the minimizer α_n^χ can be determined analytically.

3.5. Weighted L^2 Total-Variation Factor

Inspired by the edge-preserving algorithms in image restoration [4] and inverse scattering [22, 13], we now consider the TV-factor as a weighted norm on $L^2(D)$, in which the weighting favors flat parts and non-flat parts of the contrast profile almost equally. In stead of (43) we choose the TV-factor as

$$F_n^{\mathrm{TV}}(\chi) = \frac{1}{V}\int_D \frac{|\nabla\chi(\boldsymbol{q})|^2 + \delta_{n-1}^2}{|\nabla\chi_{n-1}(\boldsymbol{q})|^2 + \delta_{n-1}^2}\mathrm{dv}(\boldsymbol{q})\,, \tag{50}$$

where $V = \int_D \mathrm{dv}(\boldsymbol{q})$ denotes the area (two-dimensional volume) of the test domain D. Similar as before $F_n^{\mathrm{TV}}(\chi_{n-1}) = 1$ and the updating scheme of the contrast sources $w_{j,n}$ and the fields $u_{j,n}$ is not changed. We note that Zhdanov and Hursan [34] used an additive regularization with a weighted norm similar to (50).

The gradient of the weighted TV-factor of (50) becomes

$$g_n^{\mathrm{TV}}(\boldsymbol{q}) = \frac{1}{V}\nabla\cdot\left[\frac{\nabla\chi_{n-1}(\boldsymbol{q})}{|\nabla\chi_{n-1}(\boldsymbol{q})|^2 + \delta_{n-1}^2}\right]. \tag{51}$$

Comparing this gradient with the one of (48), for $p = 1$, we immediately observe that these gradients are similar. Hence this new TV-factor may combine some properties of minimization of the total variation in the L^2-norm and in the L^1-norm (through its gradient).

The minimization of the multiplicative cost functional (49) can now be performed analytically. The cost functional is a fourth-degree polynomial in α, viz.,

$$\begin{aligned}\mathcal{F} = [&F_S(w_{j,n}) + F_{D,n}(w_{j,n},\chi_{n-1})\\ &+ 2\alpha\,\eta_{D,n}\mathrm{Re}\textstyle\sum_j\langle d_n u_{j,n}, \chi_{n-1}u_{j,n} - w_{j,n}\rangle_D + \alpha^2\,\eta_{D,n}\textstyle\sum_j\|d_n u_{j,n}\|_D^2]\\ &\times[1 + 2\alpha\,\mathrm{Re}\langle b_{n-1}\nabla\chi_{n-1}, b_{n-1}\nabla d_n\rangle_D + \alpha^2\,\|b_{n-1}\nabla d_n\|_D^2]\,,\end{aligned} \tag{52}$$

where

$$b_{n-1} = V^{-\frac{1}{2}}\left(|\nabla\chi_{n-1}|^2 + \delta_{n-1}^2\right)^{-\frac{1}{2}}\,. \tag{53}$$

Differentiation with respect to α yields a cubic equation with one real root and two complex conjugate roots. The real root is the desired minimizer α_n^χ.

In our numerical examples we use this new TV-factor as the multiplicative regularization of the CSI method and we denote this method as the MR-CSI method.

4. ROOT TEST

Before we discuss the reconstruction with the CSI and MR-CSI methods we investigate whether the solution converges to a false local minimum. To investigate this, in each iteration, we construct a direction

$$\begin{aligned} \Delta w_{j,n} &= w_j^{\text{exact}} - w_{j,n}\,, \quad j = 1, 2, \ldots\,, \\ \Delta \chi_n &= \chi^{\text{exact}} - \chi_n\,, \end{aligned}$$

where $w_{j,n}^{\text{exact}}$ is our numerical solution of the forward problem for given χ^{exact}. We then consider a variation in this direction as

$$\begin{aligned} w_j &= w_j^{\text{exact}} + \beta \Delta w_{j,n}\,, \quad j = 1, 2, \ldots\,, \\ \chi &= \chi_{\text{exact}} + \beta \Delta \chi_n\,. \end{aligned}$$

Following the analysis of Section 3.1 we observe that, besides the absolute minimum at $\beta = 0$, there exists a false minimum at

$$\beta_n = \frac{-3B_{D,n} - \sqrt{9B_{D,n}^2 - 8A_{D,n}(C_{S,n} + C_{D,n})}}{4A_{D,n}}\,. \tag{54}$$

The quantities $A_{D,n}$, $B_{D,n}$, $C_{S,n}$ and $C_{D,n}$ are obtained from (14)–(17) by substituting the quantities obtained in the n^{th} iteration. Hence, along our particular direction, there is no false minimum, when the following root test, cf. (19),

$$R_n = \frac{9B_{D_n}^2}{8A_{D,n}(C_{S,n} + C_{D,n})} < 1 \tag{55}$$

holds. Hence, as long as this root test remains satisfied, with increasing iterations, the present scheme will never be trapped in a local minimum. However, due to the ill-posed nature of our inverse problem, it is still possible that the scheme converges to a numerical result which is far from the exact solution. This phenomenon also occurs in case of an ill-posed linear problem. When the root test (55) is not satisfied, the scheme may converge to a false local minimum. In that case β_n should converge to -1. Finally, note that the left-hand side of (55) is always less than or equal to $9/8$.

5. NUMERICAL EXAMPLES

For our numerical examples, the test domain D consists of a square with sides of length d, while the measurement curve S is a circle.

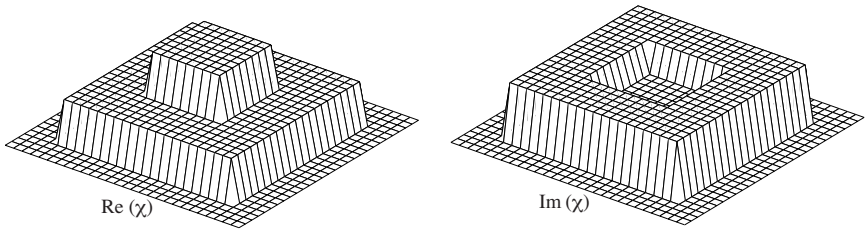

Figure 1. Original profile of concentric squares.

The homogeneous embedding is chosen to be lossless and therefore the wavenumber $k_b = 2\pi/\lambda$, where λ denotes the wavelength. The discrete form of the algorithm is obtained by dividing the test domain into subsquares, assuming the contrast, sources and fields to be piecewise constant. The integrals over subsquares are approximated by integrals over circles of equal area which are calculated analytically [24]. The discrete spatial convolutions of the operators G_D and $G_D^\star$ are computed using FFT routines [28]. The incident fields are chosen to be excited by line sources parallel to the axis of the scatterer. These sources are taken to be equally spaced on the measurement circle, and the source locations are also chosen as discretization points on the circle. All integrals on S are approximated by point collocation at the discretization points, that is, the rectangular rule with the integrand evaluated at the mid-points. The measured data are simulated by solving the direct scattering problem with the help of a conjugate gradient method [28]. The circle S is subdivided into J equally spaced arcs, each mid-point serving as the location of a line source as well as a receiver. The number of data is then equal to $J \times J$. Some numerical experiments have been carried out for the configuration, which was used to test the CSI method [32, 30].

5.1. Concentric Squares

We first consider a scattering object that consists of concentric square cylinders, an inner cylinder of dimension λ by λ, with complex contrast $\chi = 0.6+0.2i$, surrounded by an outer cylinder, 2λ by 2λ, with contrast $\chi = 0.3 + 0.4i$. The test domain D is a square of dimension $d = 3\lambda$ by $d = 3\lambda$ and is discretized into 29×29 subsquares. The circle S, where both the sources and receivers are located, has a radius of 3λ. The discretized real and imaginary parts of the exact contrast profile are shown in Figure 1.

Using the CSI method, the reconstructions after 512 iterations are shown in Figure 2, for 10, 18 and 30 source/receiver stations,

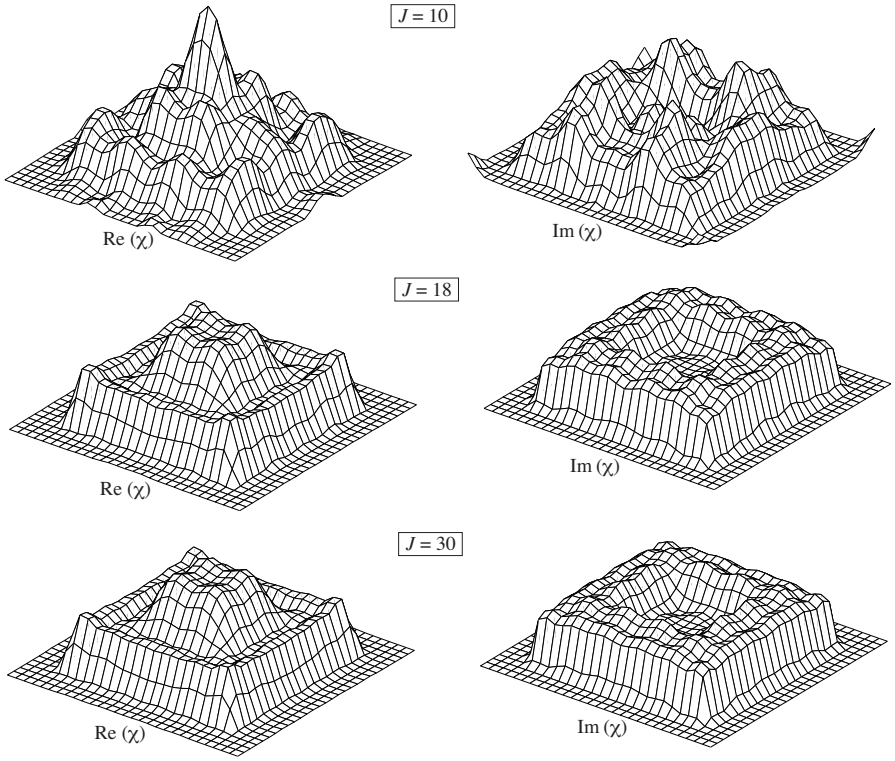

Figure 2. CSI reconstruction after 512 iterations, for various source/receiver stations: $J = 10,\ 18$, and 30.

respectively. In Figure 3 we have plotted R_n as a function of the number of iterations, n, for various numbers, J, of source/receiver stations. Using the CSI method (top figure) we observe that, for $J = 5$, 10 and 15, the value R_n of the root test converges to values larger than 1 and a false minimum can be arrived at. Further for these cases, we have observed that β_n converges to -1, which means that the scheme indeed ends up in a false minimum. For $J > 16$ we observe that the scheme does not end up in a false minimum. Using only 10 stations, Figure 3 (top) shows that we end up in a local minimum, and this is confirmed by the bad reconstruction in Figure 2 (top). However, already with 18 stations a band-limited approximation of our contrast profile is arrived at. Note that increasing the number of sources yields no further improvement, the result is the same band-limited approximation of the exact profile, and Figure 3 indicates that

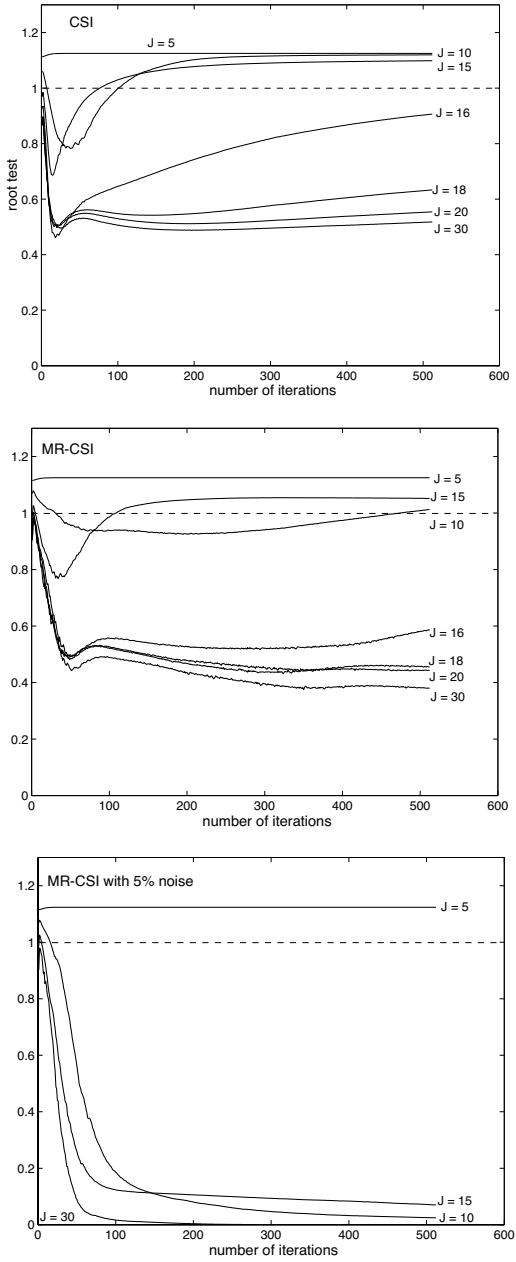

Figure 3. The quantity R_n for the CSI method (top), the MR-CSI method (middle) and the MR-CSI method with 10% noise (bottom), applied to the profile of concentric squares.

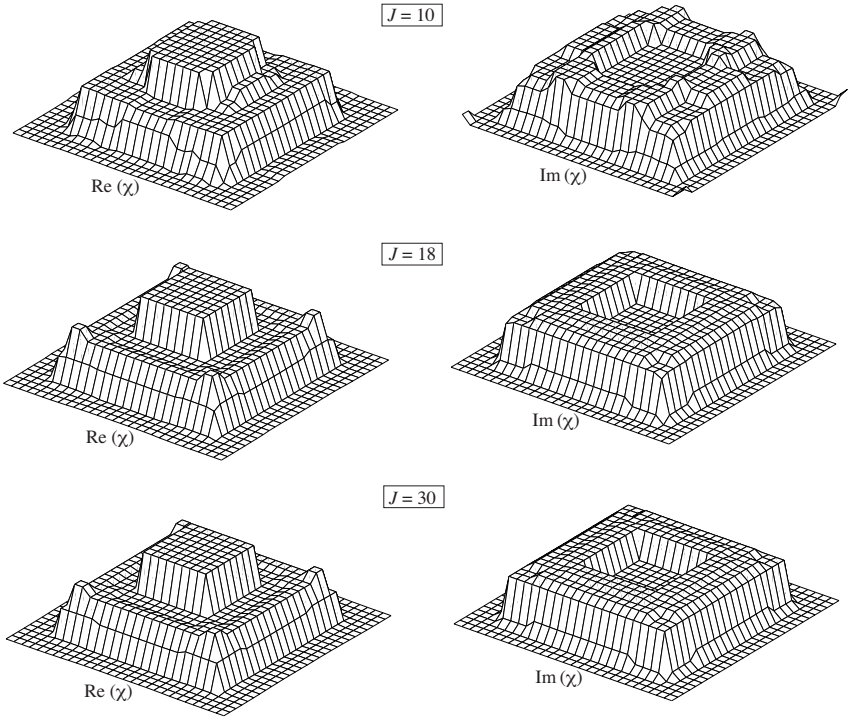

Figure 4. MR-CSI reconstruction after 512 iterations, for various source/receiver stations: $J = 10,\ 18$, and 30.

this is not a local minimum. Hence, if we are able to reduce the band-limitation in some way, we will approach the exact global minimum.

Extending the CSI method with the weighted L^2 total-variation factor to the MR-CSI method, the reconstructions after 512 iterations are shown in Figure 4, again for 10, 18 and 30 source/receiver stations, respectively. Using the MR-CSI method the pictures has improved and that is in agreement with the results shown in Figure 3 (middle). Now, using only 10 stations, Figure 4 (top) shows that we obtain a reasonable approximation of the contrast profile, but already with 18 stations we arrive at a good approximation to the exact contrast profile, while Figure 3 (middle) shows that we seem to converge to a global minimum. In fact, continuing the iterations leads to further improvement. The present regularization has reduced the band-limitation almost completely. Further, by comparing the middle and bottom pictures of Figure 4, we again observe that increasing the number of stations does not yield further improvement.

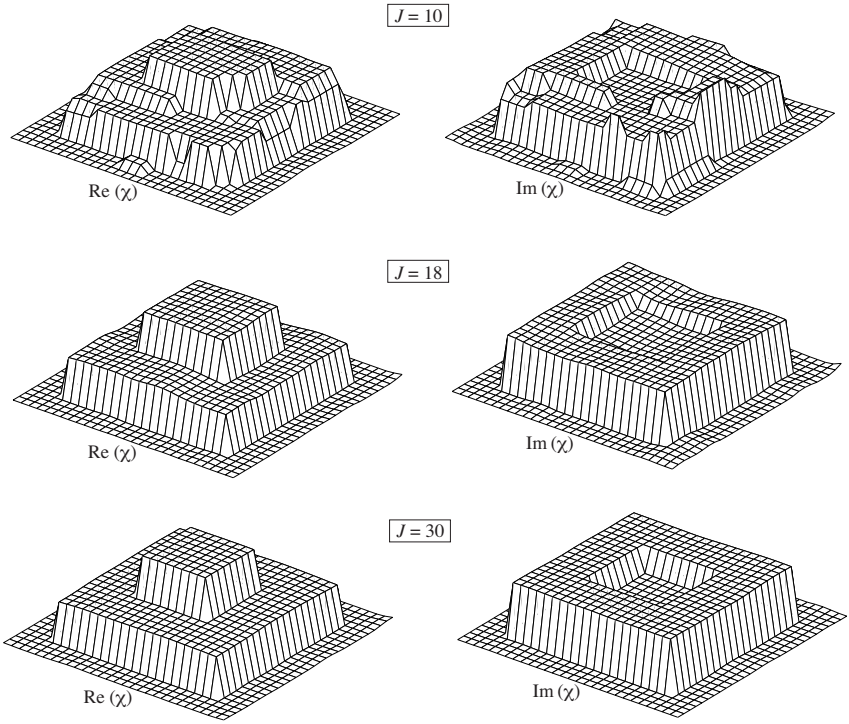

Figure 5. MR-CSI reconstruction with 10% noise after 512 iterations, for various source/receiver stations: $J = 10,\ 18$, and 30.

Finally, adding 10% white noise to the data leads to significant improvement, see Figure 5. This feature of the MR-CSI method is due to the term F_S, which takes care of a higher weighting of the TV-factor, when noise is present, while the TV-factor reduces the influence of the noise on the reconstructed profile. In case of the presence of noise, it is expected that more stations will reduce the disturbing influence of the noise on the reconstructed profiles. Increasing the number of sources from 18 to 20, leads indeed to improved reconstruction, this in contrary to the noise-free results of Figure 4. In agreement with these pictures, we also observe from Figure 3 (bottom) that the scheme with noisy data does not end up in a local minimum when $J > 10$. This established the fact that the MR-CSI method is very robust for noisy data. With this knowledge we can judge the reconstruction of other examples in more detail.

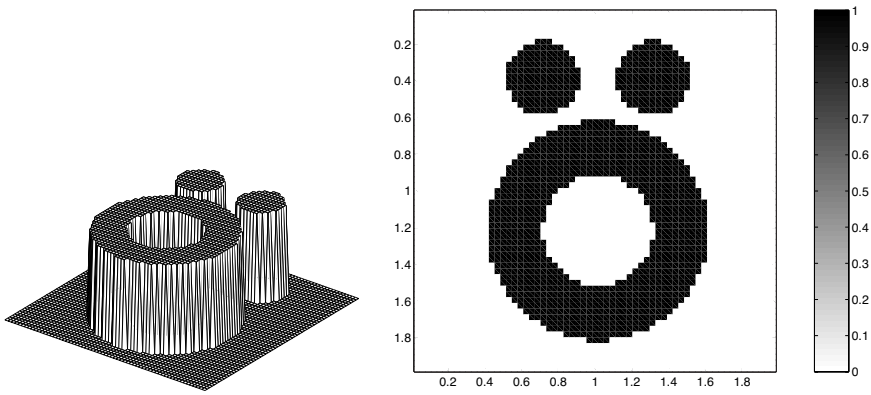

Figure 6. Original ö profile.

5.2. 'Austria' Profile

In our second example, a number of single objects are contained in a test domain of side $d = 2$ m. These objects consist of two disks and one ring. The disks of radius 0.2 m are centered at $(0.3, 0.6)$ m and $(-0.3, 0.6)$ m. The ring has an exterior radius of 0.6 m and an inner radius of 0.3 m, and is centered at $(0, 0.2)$ m. The electromagnetic case is considered, where the objects have a relative permittivity of 2 ($\chi = 1$). This ö profile is referred to as the 'Österreich' profile by Belkebir and Tijhuis [27]. They used a distorted Born method together with a 'marching-on-in frequency' technique from 100, 200, 300 to 400 MHz. For each frequency, the data were treated separately. The initial guess corresponds to the result of the last iteration of the previously treated frequency. The lower frequency gives a rough global approximation of the contrast profile, while higher frequencies increase the resolution. A similar frequency-hopping technique has been applied by Litman *et al.* [23], but using a controlled evolution of a level set for binary objects. They have used 64 sources and 65 receivers on a circle of radius 3 m centered at (0,0), while the test domain was discretized into 30×30 cells. To obtain more detail at higher frequencies, we discretize the test domain into 64×64 cells, but we take only 48 source/receiver stations. Hence, it seems that we have under sampled our problem, but the reconstructions will show that it does not reduce the quality of reconstruction. The original ö profile is presented in Figure 6, both as a surface plot and as a density plot.

In contrast to the multi-frequency inversion methods of [27] and [23], we first consider the reconstruction results of our single-frequency

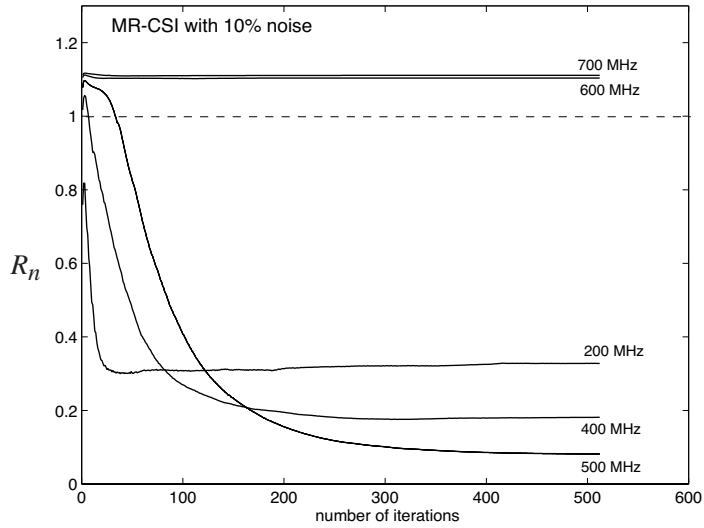

Figure 7. The quantity R_n for the MR-CSI method, with 10% noise, applied to the ö profile.

inversion method. Although we have the *a priori* information that the profile is real, we did not use this information and we reconstruct for complex contrast. However, in the figures we only present a density plot of the real part of the contrast. Further, we have distorted our data with 10% noise.

In Figure 7, the quantity R_n of the left-hand side of (55) has been plotted as a function of the number of iterations, for various frequencies. From this figure we may conclude that, for frequencies of 200, 400 and 500 MHz, the results converge to the global minimum, while the results for frequencies of 600 and 700 MHz converge to a false minimum. Indeed, for the latter cases, the value of β_n converges to -1. This phenomenon is confirmed by the actual reconstructions in Figure 8 after 512 iterations. We observe that for 200 to 500 MHz good reconstructions are obtained, while the resolution increases with increasing frequency. For these cases, the imaginary parts of the contrast were very small. However, for the cases of 600 MHz ($d = 4\lambda$) and 700 MHz ($d = 4\frac{2}{3}\lambda$), there is no real reconstruction and the imaginary parts of the contrast appear to be very large. This confirms again that for the latter frequencies we are trapped in a false local minimum.

On the other hand, when we use the results of 500 MHz as initial guess for a single-frequency inversion at 700 MHz (frequency hopping

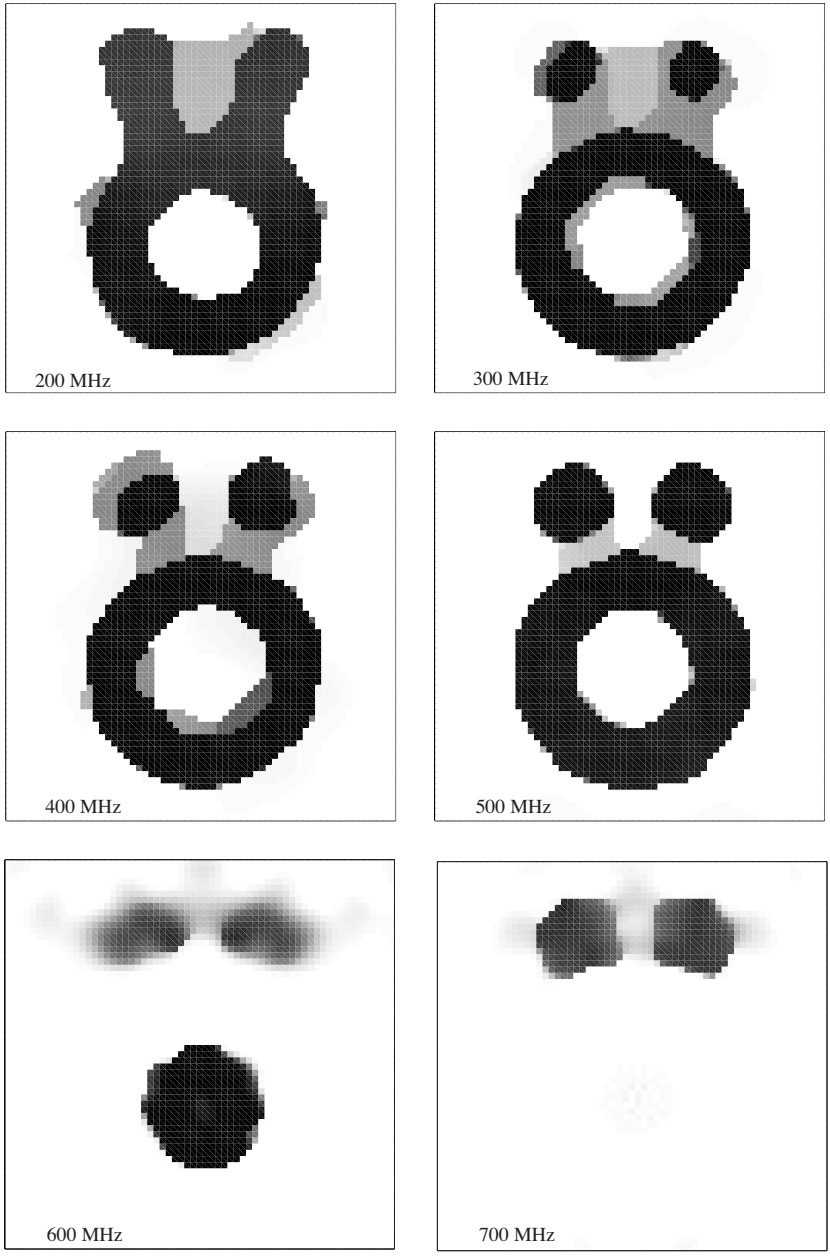

Figure 8. MR-CSI reconstruction with 10% noise, $f = 200,\ 300,\ 400,\ 500,\ 600,\ 700$ MHz.

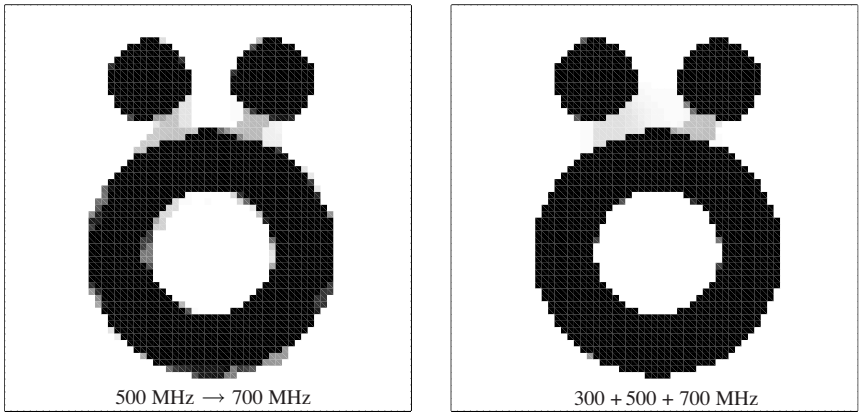

Figure 9. MR-CSI reconstruction with 10% noise using frequency-hopping from 500 MHz to 700 MHz after 512 iterations (left) and using the frequencies 300, 500 and 700 MHz simultaneously after 1024 iterations (right).

from 500 MHz to 700 MHz), we obtain the reconstruction results presented in Figure 9 (left picture). Although this result is obtained using only 32×32 source/receiver stations and 512 iterations, we immediately observe that the resolution has been improved.

In stead of frequency hopping we also implement the present multiplicative regularization in an algorithm dealing with a number of frequencies, simultaneously. We then use the Maxwell model for the representation of the contrast as a function of the frequency, as it is described in [32]. We leave out further details, but we remark that in this multi-frequency case, we have to operate with frequency dependent update parameters for the updating of the contrast sources [32]. In view of the larger complexity of the multi-frequency inversion problem, the rate of convergence of the algorithm has been decreased and therefore we carry out 1024 iterations. The reconstruction results are shown in the right picture of Figure 9. Comparing the frequency hopping method (left) and the multi-frequency method (right), we again observe improved resolution and the differences with the exact profile of Figure 6 are very small, notwithstanding the 10% noise added to the data. Although it is computationally more expensive to perform a simultaneous inversion for the frequencies at hand, the risk to end up in a false minimum has been reduced.

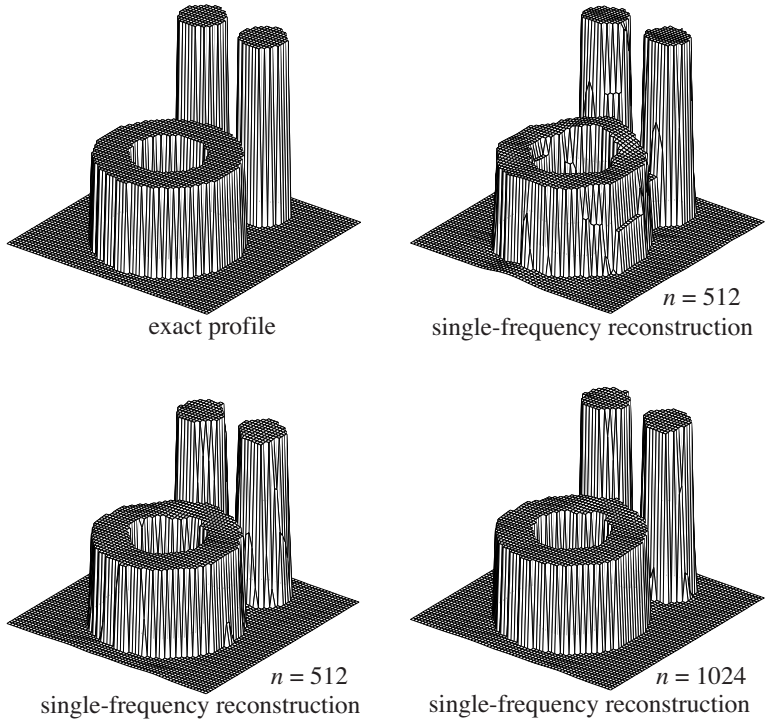

Figure 10. Exact profile (left-top), and MR-CSI reconstructions with 10% noise using a single frequency of 500 MHz, after 512 iterations (right-top) and using the frequencies 300, 500 and 700 MHz simultaneously, after 512 iterations (left-bottom) and after 1024 iterations (right-bottom).

5.3. Extended 'Austria' Profile

For a further test of our MR-CSI method, we again consider the ö profile, but we take the relative permittivity of the two disks such that the contrast is twice as large ($\chi = 2$). The exact profile of this extended ö is presented in the left-top picture of Figure 10. It clearly shows that we are now dealing with a more complex contrast profile. We take the scattered field data at 32 source/receiver stations. Again we add 10% noise to these data. In the first instance we consider a single frequency of 500 MHz. The reconstruction after 512 iterations is presented in the right-top picture of Figure 10. Although the reconstruction is very good, we perform also a multi-frequency inversion, using the data at 300, 500 and 700 MHz, simultaneously.

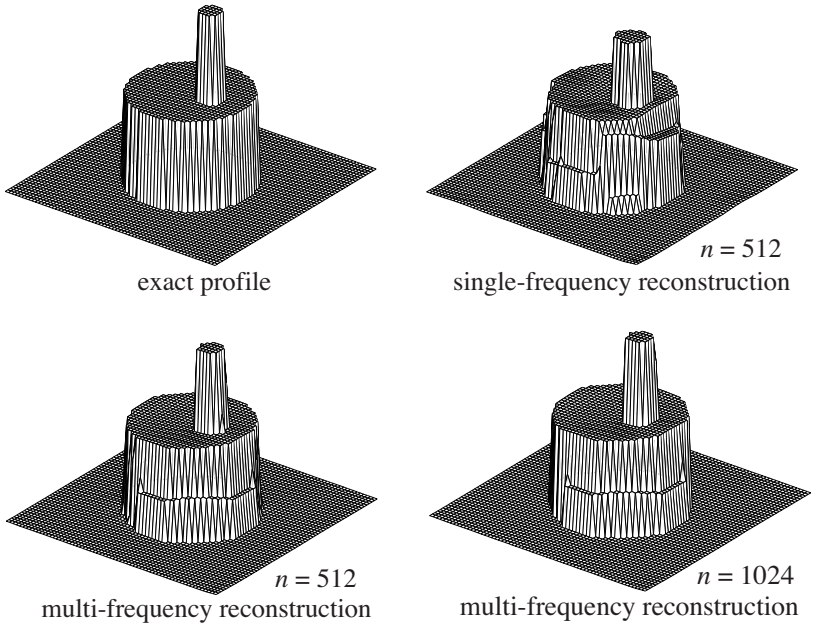

Figure 11. Exact profile (left-top), and MR-CSI reconstructions with 10% noise using a single wavenumber of 7, after 512 iterations (right-top) and using the wavenumbers 5, 7 and 9, simultaneously, after 512 iterations (left-bottom) and after 1024 iterations (right-bottom).

The result after 512 iterations is shown in the left-bottom picture, while the result after 1024 iterations is presented in the right-bottom picture. We observe that the resolution improves using the multi-frequency inversion, certainly after 1024 iterations. The difference with the exact profile is almost invisible to the naked eye.

5.4. 'Finger' Profile

As last example we consider the 'finger' profile, used by Colton and Monk [10] in an acoustic inversion problem. In a test domain of $d = 2$ m a circular cylinder with radius 0.6 m is centered. The index of refraction is 2; this means that the contrast is equal to one. This cylinder is perturbed: a small cylinder with contrast $\chi = 2$ is present with origin at $(\frac{1}{3}, 0)$ m. The radius of this circular perturbation is 0.1 m. Colton and Monk [10] used scattered data at different wavenumbers, viz. data at the four wavenumbers k_{b} =1, 3, 5 and 7 m^{-1}. The number of incident waves for each value of k_{b} was 51.

In our inversion procedure, we take only 32 source/receiver stations and we consider either the single-frequency inversion with wavenumber $k_b = 7$ m^{-1} ($d = 2.2\lambda$) or the multi-frequency inversion with the three wavenumbers $k_b = 5$, 7 and 9 m^{-1}. Although Colton and Monk used a circular test domain, we take a square test domain with side length $d = 2$ m and discretized into 64×64 subsquares. The left-top picture of Figure 11 shows the exact profile, while the right-top picture represents the single-frequency reconstruction after 512 iterations. Note that for this single-frequency case we already have a good reconstruction, although the 'finger' is a little too short and too thick. The multi-frequency reconstruction yields after 512 iterations (left-bottom picture) a more slender 'finger', while increasing the number of iterations up to 1024 (right-bottom picture) increases its length.

6. CONCLUSIONS

We have discussed a new type of regularization that together with the contrast source inversion method leads to a very effective inversion technique for various applications. The multiplicative regularization avoids the *a priori* knowledge about the material composition and shape of the unknown object substantially. The artificial tuning process, with a weighting parameter of the regularization to obtain the 'cosmetically best' result, seems superfluous. A new type of edge-preserving regularization has been introduced, being a weighted L^2-norm, so that the update parameters can be determined explicitly, avoiding the usual line minimization for finding the optimum parameter.

We have treated in detail the two-dimensional problem. The extension to a full 3D electromagnetic problem is under development. In this context we refer to [2], where the contrast source inversion method for a full vectorial 3D electromagnetic problem has been discussed, and where a multiplicative regularization has been employed using the L^1-norm, see (43) for $p = 1$. The introduction of the new weighted L^2-norm as regularization factor will simplify the updating of the contrast significantly, while we expect improved reconstruction.

ACKNOWLEDGMENT

The authors thank Dr. N. V. Budko and Dr. R. F. Remis for their stimulating discussions about the occurrence of local minima in the contrast source inversion method.

REFERENCES

1. Abubakar, A. and P. M. van den Berg, "Nonlinear inversion in electrode logging in a highly deviated formation with invasion using an oblique coordinate system," *IEEE Trans. Geosci. Remote Sensing,* Vol. 38, 25–38, 2000.
2. Abubakar, A., P. M. van den Berg, and B. J. Kooij, "A conjugate gradient contrast source technique for 3D profile inversion," *IEICE Trans. Electron.,* E83-C, 1864–1874, 2000.
3. Acar, R. and C. R. Vogel, "Analysis of bounded variation penalty methods for ill-posed problems," *Inverse Problems,* Vol. 10, 1217–1229, 1994.
4. Charbonnier, P., L. Blanc-Féraud, G. Aubert, and M. Barlaud, "Deterministic edge-preserving regularization in computed imaging," *IEEE Trans. Image Process.,* Vol. 6, , 298–311, 1996.
5. Blomgren, P., T. F. Chan, P. Mulet, and C. K. Wong, "Total variation image restorations: numerical methods and extensions," *IEEE Proc. ICIP 97,* 384–387, 1997.
6. Chan, T. F. and C. K. Wong, "Total variation blind deconvolution," *IEEE Trans. on Image Processing,* Vol. 7, 370–375, 1998.
7. Chew, W. C., "Complexity issues in inverse scattering problems," *Proceedings of Antennas and Propagation Society, IEEE International Symposium,* Vol. 3, 1627, 1999.
8. Colton, D., J. Coyle, and P. Monk, "Recent developments in inverse acoustic scattering theory," *Siam Review,* Vol. 42, 369–414, 2000.
9. Colton, D. and R. Kress, *Inverse Acoustic and Electromagnetic Scattering Theory,* Springer, Berlin, 1992.
10. Colton, D. and P. Monk, "The numerical solution of an inverse scattering problem for acoustic waves," *IMA Journal of Applied Mathematics,* Vol. 49, 162–184, 1992.
11. Dobson, D. C. and F. Santosa, "An image-enhancement technique for electrical impedance tomography," *Inverse Problems,* Vol. 10, 317–334, 1994.
12. Dobson, D. C. and F. Santosa, "Recovery of blocky images for noisy and blurred data," *SIAM Journal of Applied Mathematics,* Vol. 56, 1181–1198, 1996.
13. Dourthe, C., Ch. Pichot, J. Y. Dauvignac, L. Blanc-Féraud, and M. Barlaud, "Regularized bi-conjugate gradient algorithm for tomographic reconstruction of buried objects," *IEICE Trans. Electron.,* Vol. E83-C, 1858–1863, 2000.

14. Habashy, T. M., M. L. Oristaglio, and A. T. de Hoop, "Simultaneous nonlinear reconstruction of two-dimensional permittivity and conductivity," *Radio Science,* Vol. 29, 1101–1118, 1994.
15. Hansen, P. C., "Analysis of discrete ill-posed problems by means of the L-curve," *SIAM Review,* Vol. 34, 561–580, 1992.
16. Isernia, T., V. Pascazio, and R. Pierri, "On the local mimina in a tomographic imaging technique," *IEEE Trans. Geosci. Remote Sensing,* to appear.
17. Kleinman, R. E. and P. M. van den Berg, "A modified gradient method for two-dimensional problems in tomography," *J. Computat. Appl. Math.,* Vol. 42, 17–35, 1992.
18. Kleinman, R. E. and P. M. van den Berg, "An extended range modified gradient technique for profile inversion," *Radio Science,* Vol. 28, 877–884, 1993.
19. Kleinman, R. E. and P. M. van den Berg, "Two-dimensional location and shape reconstruction," *Radio Science,* Vol. 29, 1157–1169, 1994.
20. Kohn, R. V. and A. McKenney, "Numerical implementation of a variational method for electrical impedance tomography," *Inverse Problems,* Vol. 6, 389–414, 1990.
21. Lesselier, D. and B. Duchêne, "Wavefield inversion of objects in stratified environments. From backpropagation schemes to full solutions," *Review of Radio Science, 1993–1996,* R. Stone (ed.), 235–268, Oxford University Press, Oxford, 1996.
22. Lobel, P., L. Blanc-Féraud, Ch. Pichot, and M. Barlaud, "A new regularization scheme for inverse scattering," *Inverse Problems,* Vol. 13, 403–410, 1997.
23. Litman, A., D. Lesselier, and F. Santosa, "Reconstruction of a two-dimensional binary obstacle by controlled evolution of a level-set," *Inverse Problems,* Vol. 14, 685–706, 1998.
24. Richmond, J. H., "Scattering by a dielectric cylinder of arbitrary cross section shape," *IEEE Trans. Antennas and Propagation,* Vol. 13, 334–341, 1965.
25. Rudin, L., S. Osher, and C. Fatemi, "Nonlinear total variation based noise removal algorithm," *Physica,* Vol. 60D, 259–268, 1992.
26. Sabatier, P. C., "Past and future of inverse problems," *J. Math. Phys.,* Vol. 41, 4082–4124, 2000.
27. Belkebir, K. and A. G. Tijhuis, "Using multiple frequency information in the iterative solution of a two-dimensional non-linear inverse problem," *Proc. PIERS 96: Progress In Electromagnetic Research Symposium,* 353, Innsbruck, Austria,

1996.

28. Van den Berg, P. M., "Iterative computational techniques in scattering based upon the integrated square error criterion," *IEEE Trans. Antennas and Propagation,* Vol. 32, 1063–1071, 1981.
29. Van den Berg, P. M., "Non-linear scalar inverse scattering: algorithms and applications," *Scattering,* R. Pike and P. C. Sabatier (eds.), Chapter 1.3.3., Academic Press, London, 2001, to appear.
30. Van den Berg, P. M., A. L. van Broekhoven, and A. Abubakar, "Extended contrast source inversion," *Inverse Problems,* Vol. 15, 1325–1344, 1999.
31. Van den Berg, P. M. and R. E. Kleinman, "A total variation enhanced modified gradient algorithm for profile reconstruction," *Inverse Problems,* Vol. 11, L5–L10, 1995.
32. Van den Berg, P. M. and R. E. Kleinman, "A contrast source inversion method," *Inverse problems,* Vol. 13, 1607–1620, 1997.
33. Vogel, C. R. and M. E. Oman, "Iterative methods for total variation denoising," *SIAM Journal of Scientific Computing,* Vol. 17, 227–238, 1996.
34. Zhdanov, M. and G. Hursan, "3D electromagnetic inversion based on quasi-analytical approximation," *Inverse Problems,* Vol. 16, 1297–1322, 2000.